An In-package EMC based Relative Humidity Sensor

Sattari, Romina; Van Zeijl, Henk; Chang, Zu Yao; Zhang, Guo Qi

DOI
10.1109/JSEN.2025.3571230

Publication date
2025

Document Version
Final published version

Published in
IEEE Sensors Journal

An In-Package EMC-Based Relative Humidity Sensor

Romina Sattari, *Member, IEEE*, Henk van Zeijl, Zu Yao Chang, *Member, IEEE*, and Guo Qi Zhang, *Fellow, IEEE*

***Abstract*—This article presents a novel in-package relative humidity (RH) sensor designed to enhance moisture detection within the chip encapsulation material, specifically epoxy molding compound (EMC). Traditional methods for assessing EMC moisture content, such as mass measurements, are time-consuming and incompatible with industrial reliability tests, limiting their use for real-time, in situ monitoring. To address these challenges, we propose an integrated capacitive sensor that directly measures moisture content within the encapsulation material. The sensor utilizes a heterogeneous electrode design to overcome the sensitivity limitations of conventional interdigital electrodes (IDEs). This design features sections of different widths, allowing selective wet chemical etching of the silicon dioxide layer using buffered hydrofluoric acid (BHF). By controlling the etching time, the silicon dioxide layer beneath the narrower sections is completely etched, while oxide pillars form under the wider sections, resulting in semifloating electrodes. The EMC fills the etched regions and wraps around the narrower sections, concentrating more electric field lines in the EMC and enhancing sensor sensitivity. Our proposed sensor achieves a capacitance change of 1 pF per 80% RH, improving sensitivity from 6.9 to 12.3 fF/%RH, with a 20% increase in relative capacitance change. A shielding layer is added to minimize parasitic capacitance effects, ensuring accurate measurements. The proposed sensor is fully CMOS-compatible and can monitor moisture-induced reliability risks, as well as assess packaging material aging. This work provides a cost-effective and reliable solution for in-package humidity monitoring in semiconductor applications.**

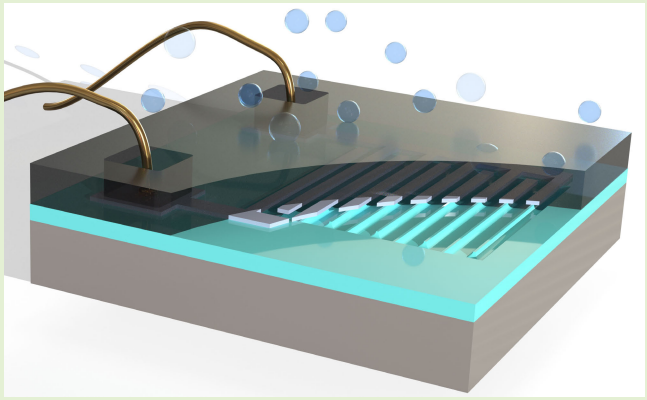

***Index Terms*— Epoxy molding compound (EMC), heterogeneous electrodes, in-package relative humidity (RH) sensor, interdigital electrodes (IDEs), packaging encapsulation material, parasitic capacitance, through-polymer rim (TPR), wet chemical etching.**

I. Introduction

MICROELECTRONIC components are introduced to an increasing number of applications as part of a control or monitoring device, as sensors, or as means of tracking. Depending on the application, extreme loading profiles may need to be endured such as high temperatures, random vibrations, or humid and even wet environments. Therefore, encapsulation materials are used to protect the electronics.

In electronic packaging, epoxy molding compounds (EMCs) are widely used as encapsulants, but their moisture absorption properties can lead to serious reliability issues such as delamination, popcorning, weakened interfacial adhesion, electrochemical migration, and mechanical property degradation. The epoxy matrix of molding compounds tends to absorb water molecules and subsequently exhibits a swelling behavior that is unique to the chemistry of epoxy. Since most of the other materials involved do not swell when exposed to moisture, stress is induced between the materials. Moisture-induced die stresses in PBGA and Quad Flat packages have been studied in [1] and [2], respectively.

An example is shown in Fig. 1, where the epoxy molding compound in semiconductor packages gradually absorbs moisture from the ambient. During device operation, heat generated by the circuit causes the absorbed moisture to vaporize, leading to internal pressure build-up. This pressure weakens interfacial

Received 19 March 2025; revised 6 May 2025; accepted 6 May 2025. Date of publication 23 May 2025; date of current version 2 July 2025. This work was supported by Delft University of Technology through the HiPer Project, which concentrates on the Development of High-Performance Vehicle Computer and Communication System for Autonomous Driving within the framework of Penta and the Dutch Authority under Project 17006. The associate editor coordinating the review of this article and approving it for publication was Prof. Bhaskar Choubey. *(Corresponding author: Romina Sattari.)*

Romina Sattari and Zu Yao Chang are with the Department of Microelectronics, Faculty of EEMCS, TU Delft, 2628 CD Delft, The Netherlands (e-mail: R.Sattari@tudelft.nl; Z.Y.Chang@tudelft.nl).

Henk van Zeijl and Guo Qi Zhang are with the Electronic Components, Technology and Materials Group, TU Delft, 2628 CD Delft, The Netherlands (e-mail: h.w.vanzeijl@tudelft.nl; g.q.zhang@tudelft.nl).

Digital Object Identifier 10.1109/JSEN.2025.3571230

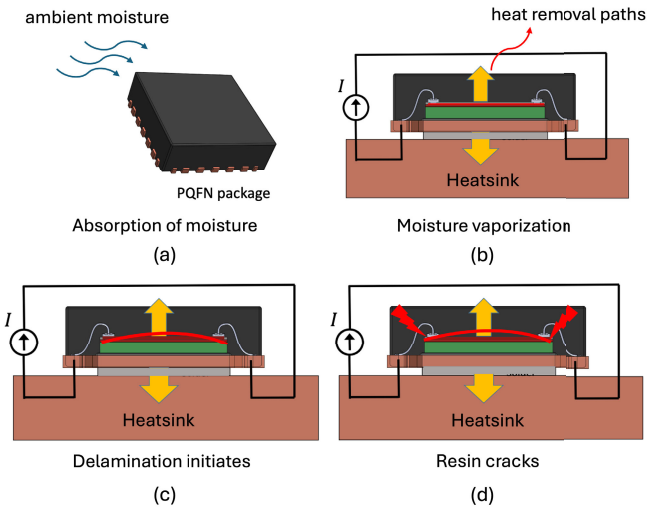

Fig. 1. Moisture-induced delamination in a PQFN package. (a) Moisture absorption from ambient air. (b) Heat during operation vaporizes moisture, creating internal pressure. (c) Delamination initiates at the die-attach interface. (d) Cracks propagate, leading to potential failure.

adhesion, initiating delamination at critical boundaries such as the EMC-to-lead frame or EMC-to-die interface. As thermal cycling continues, cracks propagate through the resin, potentially reaching the die or interconnects, resulting in electrical failure or package breakdown.

Furthermore, moisture poses a danger to the reliable performance of microelectronic devices because of corrosion when the diffusing water reaches the encapsulated electronics.

In [3], the humidity-related properties of EMC were investigated using mass measurements. However, this approach is often incompatible with industrial reliability test procedures, as it requires precise microbalance equipment, is time-consuming, and does not reflect real-time humidity sensing conditions within a packaged device. These limitations make it impractical for large-scale or in situ monitoring applications.

To effectively mitigate moisture-induced reliability concerns, real-time monitoring of EMC humidity levels is essential. However, conventional humidity sensors [4], [5] are designed for ambient conditions to measure the humidity level in the air and cannot directly assess moisture absorption within the encapsulated environment. Thus, an integrated in-package humidity sensor is required to provide direct, real-time data on EMC moisture content, enabling a more reliable assessment of package performance over time.

In general, RH sensors can be resistive or capacitive [5], [6], [7], [8]. Resistive sensors measure RH by detecting changes in a hygroscopic material's resistance, such as polymer, ceramic, or metal oxide. Moisture absorption alters resistance, which is measured using circuits such as voltage dividers or Wheatstone bridges to provide an RH output. Resistive humidity sensors are efficient in terms of manufacturing cost and process complexity. However, they may require periodic calibration to ensure accurate measurements due to nonlinearity. Moreover, their response is limited to poor sensitivity at low humidity levels below 10%, mainly due to insufficient resistance conductivity [9].

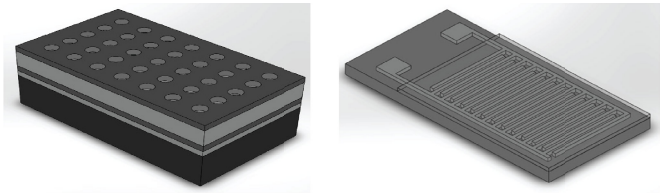

Fig. 2. (a) PP sensor. (b) Interdigital electrode (IDE) sensor coated with sensing material.

Capacitive humidity sensors measure RH by detecting changes in the dielectric constant of a sensing element. As the ambient humidity level changes, the hygroscopic material absorbs or releases moisture, which changes the dielectric constant of the sensing element. This change in the dielectric constant alters the capacitance [10], [11]. In contrast to resistive RH sensors, capacitive RH sensors respond faster and perform more accurately. Moreover, they are less prone to drift over time compared to resistive humidity sensors, which simplifies their readout circuits.

The capacitive sensor design methods can be divided into a parallel plate (PP) and an interdigital electrode (IDE), as shown in Fig. 2. PP capacitive humidity sensors consist of two metal plates separated by a hygroscopic dielectric material, such as a polymer. These sensors are relatively simple and easy to manufacture but may be more susceptible to external interference.

However, traditional parallel-plate capacitive sensors require the sensing material to be sandwiched between two electrodes, making them unsuitable for in-package humidity monitoring where the chip is coated entirely with a molding compound. In contrast, IDE capacitive sensors provide a structure that allows direct interaction with the sensing material on the top. This configuration enables real-time humidity measurement while maintaining compatibility with semiconductor packaging constraints.

IDE capacitive humidity sensors use a series of interleaved metal electrodes on a substrate, typically a silicon wafer. These electrodes can be coated with a sensing material that monitors the level of humidity. Although IDE capacitive sensors offer a suitable structure for in-package sensing, their sensitivity is inherently limited, as only half of the electric field lines interact with the dielectric sensing material [12].

Our aim is to study EMC properties in relation to moisture levels, allowing the sensor to directly monitor the moisture content within the package, address potential reliability issues, and provide real-time insights into moisture-induced degradation mechanisms, such as the weakening of interfacial adhesion. Therefore, this work addresses both challenges by developing an in-package RH sensor that not only monitors the moisture absorption and desorption behavior of the EMC but also incorporates a heterogeneous electrode design to enhance sensitivity.

In the following, we first focus on capacitive sensors with IDEs and adapt them for use as in-package humidity sensors. To achieve this, we utilized EMC, a material commonly used for semiconductor packaging, directly as the sensing

material. This was accomplished by following the standard packaging process in which the electrodes are coated with EMC. Second, to overcome the sensitivity limitation of IDE sensors, this study introduces a heterogeneous electrode design that improves the response of the in-package IDE sensor to humidity variations of the EMC, ensuring accurate detection of moisture-induced reliability risks. This improved monitoring capability helps to design more reliable semiconductor packages by preventing moisture-related failures. The fabrication of the proposed sensor is fully CMOS-compatible and ensures practical integration into the semiconductor packaging without requiring additional processing steps, making it both cost-effective and practically viable for widespread industrial use.

Furthermore, the proposed sensor has the potential to monitor the aging and dielectric properties of the encapsulation material over time, contributing to the development of advanced packaging solutions for RF applications, where the dielectric properties of the molding compound influence signal attenuation. As a result, the proposed device can serve not only as a dedicated in-package humidity sensor but also as an integral component in various electronic products.

This article extends our previous conference publication [13] by moving beyond fabrication and simulation to provide a comprehensive experimental validation. We present detailed measurement results and discussions, offering a comparative analysis of sensitivity, thermal performance, and processing yield. These insights advance our understanding of sensor optimization and highlight its practical applicability in real-world conditions.

II. Materials and Methods

This section describes the design, simulation, and fabrication steps of the proposed in-package humidity sensor. The sensing mechanism relies on variations in the dielectric constant of the EMC packaging material. This change is caused by moisture absorption and desorption, as in (1), and needs to be monitored for reliability investigations of semiconductor packages [14]. The electrodes generate an electric field that translates changes in the dielectric constant of EMC into capacitance variations. A COMSOL simulation is presented to analyze the device's behavior. The optimized sensor electrode design enhances sensitivity and overall performance

$$\epsilon = f(\mathrm{RH}). \tag{1}$$

To adapt the proposed sensor for in-package reliability monitoring, the sensor employs EMC as the dielectric sensing layer, allowing direct measurement of moisture content within the encapsulation layer. Furthermore, utilizing EMC as the dielectric material for in-package RH sensors ensures compatibility with CMOS technology, enabling monolithic integration into the standard fabrication process.

Furthermore, the proposed design aims to improve the sensitivity by increasing the relative capacitance change when EMC is exposed to moisture. We designed heterogeneous interdigital electrodes such that the electrode width changes following a specific pattern, as shown in Fig. 3.

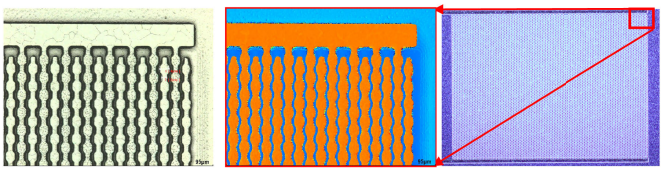

Fig. 3. Proposed heterogeneous interdigital electrodes.

In this article, we first provide a brief review of the design and manufacturing concepts of using uniform electrodes for in-package RH sensors as we proposed earlier in [15]. We then proceed to the development of an in-package humidity sensor featuring heterogeneous electrodes, highlighting how this new design improves the sensor's sensitivity. Through experimental measurements, we compare the performance of the sensor with heterogeneous electrodes with that of the uniform electrode-based sensor, demonstrating the enhanced sensitivity of the former.

A. RH Sensor With Uniform Interdigital Electrodes

In the conventional design of IDE capacitive sensors, the electrodes have a uniform structure with a consistent width or geometry throughout their entire structure. Therefore, when coated with EMC, only half of the electric field lines pass through the EMC as the target sensing layer. The remaining field lines pass through the underlying silicon dioxide insulation layer, thereby limiting the sensitivity of the IDE sensor. In our previous study, we utilized wet chemical etching to create undercuts in the silicon dioxide layer beneath the sensor electrodes, thereby increasing the contact area between the EMC and the electrodes, which enhances the sensor's sensitivity.

B. RH Sensor With Heterogeneous Interdigital Electrodes

In this work, we present a heterogeneous electrode design where the electrode's geometry varies, featuring distinct sections with different widths. This design creates regions of narrow and wide electrode lines, allowing for selective etching of the silicon oxide layer underneath. By controlling the wet chemical etching process, particularly with buffered hydrofluoric acid (BHF), we take advantage of its isotropic etching behavior, which etches the silicon dioxide at a uniform rate in all directions. By carefully controlling the etching time, we can ensure that the oxide beneath the narrower sections of the electrode is completely etched, while, beneath the wider sections, oxide pillars are formed. This results in partially free-standing or semifloating electrodes, where the EMC can fill the etched parts and completely wrap around the narrower parts. Therefore, it confines more of the electric field lines between the electrodes to pass through the EMC.

A shielding layer is used to minimize the effect of parasitic capacitance of both electrodes through silicon dioxide. This Al layer is grounded by its dedicated contact pad. In the back-end CMOS process, the last metal layer can be used to create the electrodes. The interdigital electrodes are then coated with EMC as a dielectric material between two conductors.

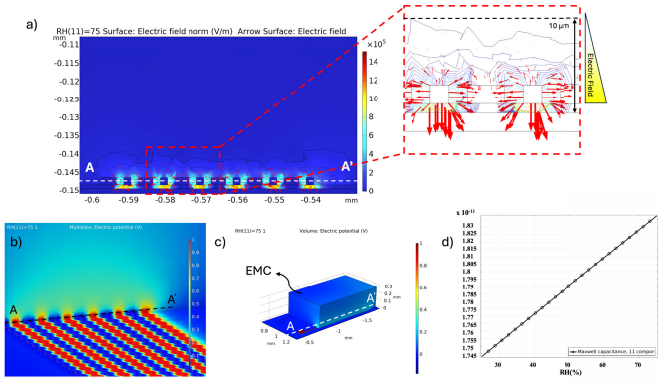

Fig. 4. Simulation in COMSOL Multiphysics. (a) Fringing field study shown with surface arrows, electric field norm, and field contours. (b) Electric potential of the electrodes. (c) 3-D simulation domain. (d) Maxwell capacitance change versus RH.

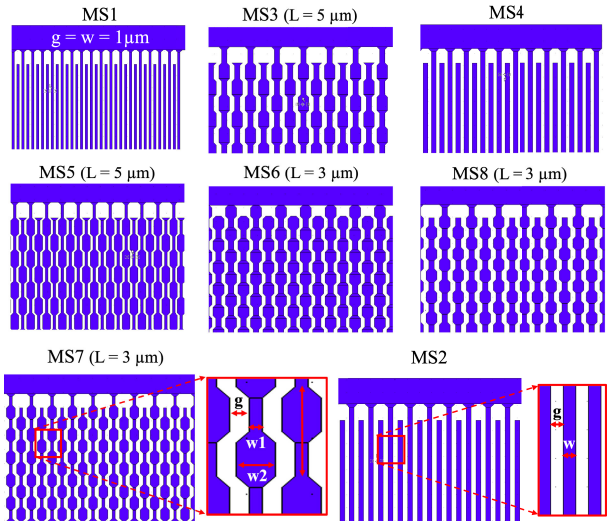

Fig. 5. Partial layout of the moisture sensors (MS) with heterogeneous and uniform electrodes.

To further illustrate the effects of moisture uptake, we simulated the sensor in COMSOL Multiphysics. Fig. 4(c) and (d) shows the simulation domain in three dimensions and the Maxwell capacitance change versus RH, respectively. Fig. 4(a) illustrates fringing field study shown with surface arrows, electric field norm, and field contours. The electric potential has also been reported in Fig. 4(b). Due to the symmetrical pattern of the electrodes, only five electrode pairs have been considered in the model to simplify the meshing grids and reduce the simulation time. The IDEs are covered with EMC as the target packaging material. Furthermore, the shielding layer is modeled as a thin-film structure with its potential set to zero, consistent with real-world conditions where the shielding electrode is connected to the ground. The effect of moisture is inherently incorporated into the dielectric change of the molding compound (EMC) itself. The dielectric constant of the EMC increases with moisture uptake, which is integrated into the simulation by an experimental equation derived from the literature. Therefore, the results cannot be directly compared with the experimental results since the EMC material properties are not identical. The purpose of the simulation is just to show the concept of a linear capacitance change with the RH level and to describe the fringe field around the electrodes.

Several heterogeneous designs with different dimensions and pitches have been manufactured and tested to optimize the design and compare with conventional uniform electrodes. The electrodes have a total length of 445 μm. The detailed dimensions are illustrated in Fig. 5 and Table I.

C. Fabrication Process Flow

The fabrication process flow is systematically illustrated in Fig. 6. The process begins with cleaning the wafer and etching lithographic alignment markers onto silicon wafers. A metal shielding layer is then deposited to create a ground layer beneath the sensor electrodes, minimizing parasitic capacitance and enhancing the relative capacitance change, thereby improving sensitivity. For this purpose, a 500-nm-thick aluminum (Al) layer is sputtered at 25 °C, chosen to ensure optically flat layers rather than optimal step coverage. Next, a 2-μm silicon dioxide layer is deposited using plasma-enhanced chemical vapor deposition (PECVD) as the insulation layer. The contact via of the shielding layer is then opened using reactive ion etching (RIE).

The heterogeneous electrodes are created by patterning a 2-μm-thick sputtered Al layer, as shown in Fig. 6(a). However, any metal compatible with the CMOS back-end metallization process can also be used. The photolithography process begins with coating the wafer with photoresist (PR), as shown in Fig. 6(b), followed by UV exposure and development of the PR to define the pattern, as detailed in Fig. 6(c). Fig. 6(d) shows the patterning of heterogeneous metal electrodes by RIE. The underlying silicon dioxide layer is then etched using BHF, as shown in Fig. 6(e). Taking advantage of the isotropic etching behavior of BHF, which removes silicon dioxide uniformly in all directions, the etching time is carefully adjusted to ensure that the oxide beneath the narrower sections of the electrode is fully etched, while oxide pillars remain beneath the wider sections. This results in partially free-standing or semifloating electrodes, allowing the EMC to fill the etched regions and completely surround the narrower sections. As a result, more electric field lines are confined within the sensing material, thereby enhancing the sensor's sensitivity.

To precisely adjust the etching time used in step F, a test procedure is defined, as shown in Fig. 7. A 2-μm silicon dioxide layer is deposited on several test wafers, and a 3.1-μm photoresist layer is patterned to match the electrode layout. The test wafers are then exposed to wet chemical etching for different time intervals, with the timing depending on the electrode dimensions and the desired depth of the side undercuts. Since the photoresist is transparent, the free-standing silicon dioxide pillars are visible under optical microscopy. After PR removal, we checked the remaining oxide pillars with SEM imaging. The data obtained from these tests can be used to fine-tune the etching time required for the main wafers.

TABLE I
SUMMARY OF THE SENSORS' SPECIFICATIONS AND MEASUREMENT RESULTS

Parameters	MS1	MS2	MS3	MS4	MS5	MS6	MS7	MS8	MS9
Capacitance before molding (pF)	3.6	0.98	0.72	1.54	2.22	1.16	1.33	0.74	0.74
Capacitance after molding (pF)	14.5	3.95	3.13	5.85	8.61	4.95	5.61	3.24	3.22
Conductance before molding (Ω^{-1})	$1.18e^{-10}$	$1.57e^{-10}$	$2.16e^{-10}$	$1.25e^{-10}$	$6e^{-12}$	$4.13e^{-12}$	$6.13e^{-11}$	$7e^{-12}$	$1.69e^{-10}$
Conductance after molding (Ω^{-1})	$2.11e^{-9}$	$2.5e^{-9}$	$2.7e^{-9}$	$4.25e^{-9}$	$4.3e^{-9}$	$1.6e^{-9}$	$3.1e^{-9}$	$6.4e^{-10}$	$2.3e^{-9}$
Layout grating pitch (g) (μm)	1	2	2	1.5	1	1.5	1.5	2	2
Layout grating width/s (w1/w2) (μm)	1	2	2/4	2	1/3	2/4	1/3	2/4	2/4
Processing yield	3/6	5/6	4/6	4/6	4/6	5/6	4/6	6/6	6/6
Sensitivity (fF/%RH)	23.4	4.5	4	6.4	12.3	6.7	7.5	4.1	4.2

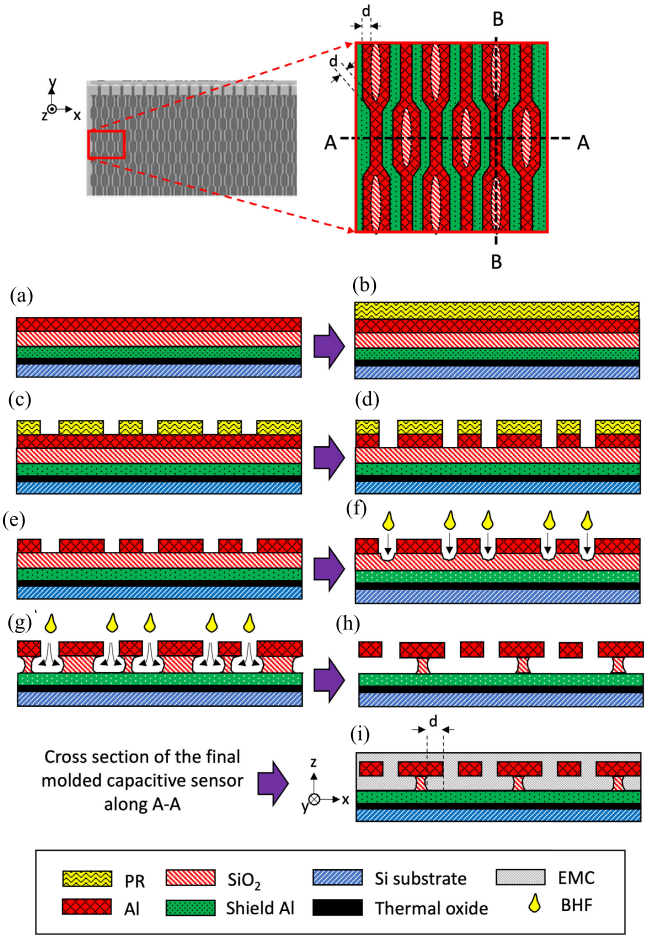

Fig. 6. Fabrication process of in-package RH sensor with heterogeneous electrodes. (a) Deposition of the 500-nm aluminum shielding layer sputtered at 25 °C followed by deposition of 2-μm silicon dioxide by PECVD. (b) Coating the structure with photoresist (PR) as a preparatory step for photolithography. (c) UV exposure and development to define the PR pattern. (d) RIE of Al heterogeneous electrodes. (e) Stripping of the photoresist using plasma treatment. (f) Isotropic etching of the underlying silicon dioxide layer using BHF. (g) Controlled etching process continued until the desired structure was achieved. (h) Final profile of the etched structure, showing partially free-standing or semifloating heterogeneous electrodes. (i) Wafer-level packaging where the electrodes are coated with EMC to fill the etched regions.

The manufacturing steps are further illustrated with SEM imaging of the device under process at each stage, as shown in Fig. 8. The final cross-sectional schematic of the device is shown in Fig. 9.

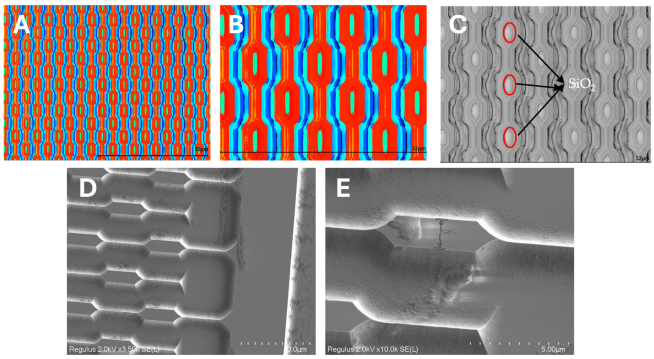

Fig. 7. Test procedure to adjust the etching time. (a) and (b) Optical imaging of the test wafer after etching in BHF for 6 min. (c) Laser imaging of the wafer after etching showing oxide pillars below the PR. (d) and (e) SEM imaging of the remained oxide pillar after PR removal.

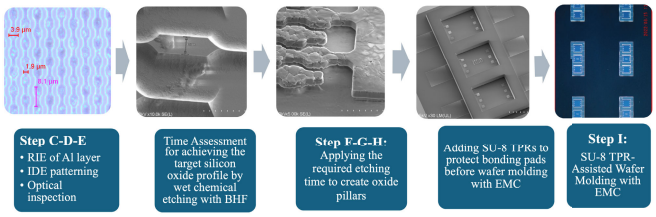

Fig. 8. SEM images illustrating the device at each processing stage, corresponding to the steps in the fabrication flowchart.

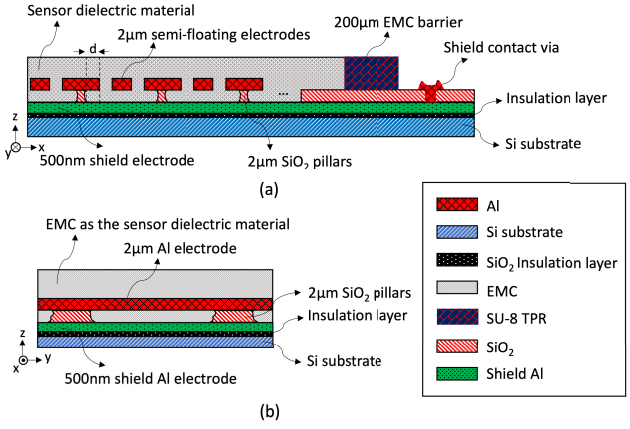

Fig. 9. Final cross-sectional schematic of the device (a) along line A-A', illustrating key structural components and (b) along line B-B'.

We also developed sensors with uniform interdigital electrodes to compare their performance with the new design.

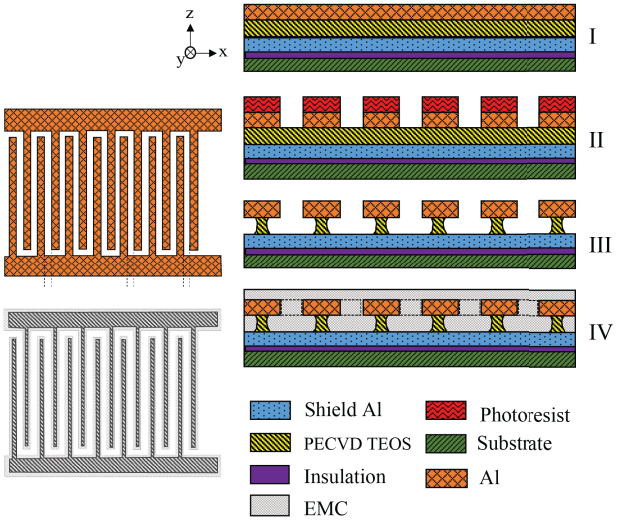

Fig. 10. Fabrication process of the in-package RH sensor with uniform electrodes.

The process flow for these sensors is shown in Fig. 10. As described in steps III and IV, the underlying silicon dioxide was over-etched using wet chemical etching, creating undercuts along the horizontal direction. These undercuts provide additional space for the EMC to flow around the metal fingers, enhancing the sensor's performance.

This capacitor, compared to the conventional sensor with uniform electrodes, is particularly advantageous since some parts of the electrodes do not have an insulating layer directly below it, meaning that in those intermediate free-standing spaces, there is extra room for encapsulation material to flow around the electrodes, so the capacitive sensor can precisely sense the properties of the molding compound. The design maximizes the electric field lines passing through the EMC.

D. Manufacturing of SU-8 Rims to Protect the Bonding Pads

To proceed with further wafer processing, the wafers must be coated with EMC during the molding process. However, the wafer-level packaging (WLP) process would completely cover the wafer, including the bonding pads. To protect these pads before molding, we introduced an additional step to create through-polymer rims (TPRs) around the pad areas with a height of 200 μm. These enclosing rims were formed using SU-8 3050, as shown in Fig. 11. SU-8 is a commonly used photosensitive, epoxy-based negative photoresist [16]. The 200-μm-thick SU-8 3050 was manually coated in two successive steps to achieve a uniform thickness within the range of ± 10 μm, which is necessary for successful WLP.

During each step, manual coating, baking, exposure, and development have been performed to create through-polymer rims. Soft baking was done at 95 °C for 45 min after each spin-coating step. To reach the acceptable layer uniformity for a successful WLP, the outer ring of the wafer was

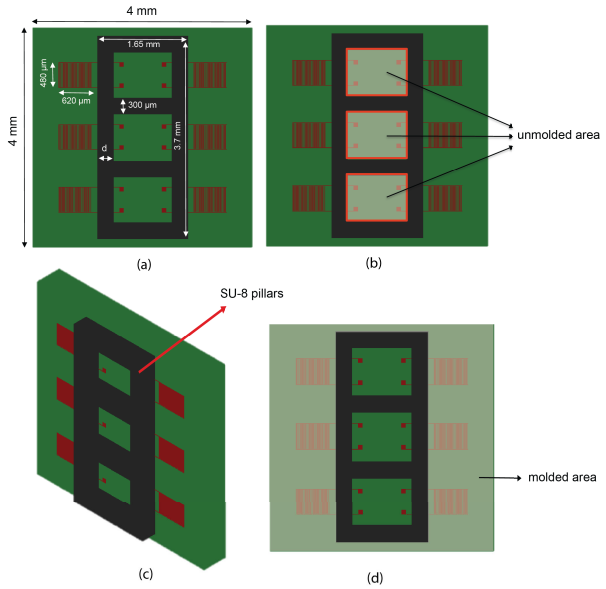

Fig. 11. RH sensor chip layout comprising. (a) SU-8 enclosing rims. (b) Unmolded area is highlighted. (c) 3-D sketch of the chip. (d) Molded area is highlighted.

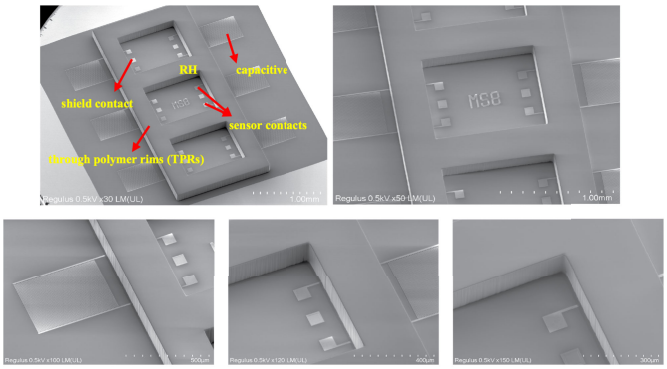

Fig. 12. SEM imaging of RH sensors and SU-8 rims.

excluded from the exposure, which creates the most thickness nonuniformity. After ultraviolet (UV) exposure for 120 s, the postexposure bake (PEB) was carried out at 65 °C for 1 min and 95 °C for 5 min. Therefore, exposed parts were cross-linked, and unexposed parts were removed by propylene glycol methyl ether acetate (PGMEA) during 20-min-long development. Finally, the patterned layer was hard-baked at 150 °C for 2 h. The SEM imaging of the processed SU-8 TPRs after hard-baking is illustrated in Fig. 12.

E. Molding Process Flow

The structure is then molded by EMC as the sensing dielectric material. In order to provide sufficient space for the EMC to flow completely between the SU-8 rims, the center-to-center pitch 6 mm is considered between the dies. The final wafer layout is illustrated in Fig. 13, and the process flow is described in Fig. 14. The molding process has been carried out by Boschman B.V., The Netherlands. The results are shown in more detail in Fig. 15.

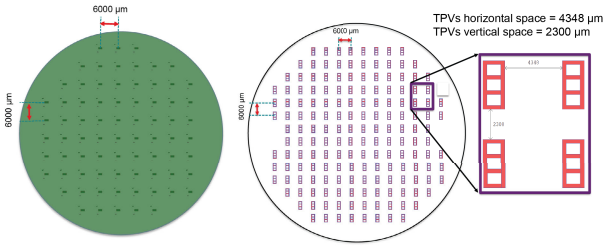

Fig. 13. 100-mm wafer layout with 6-mm pitch size.

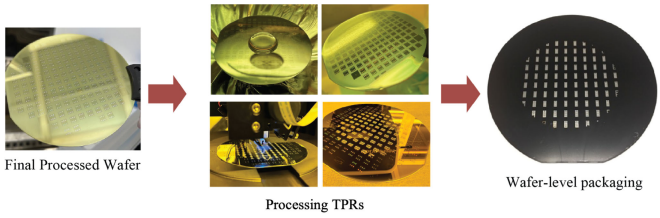

Fig. 14. Processing TPRs before wafer-level packaging.

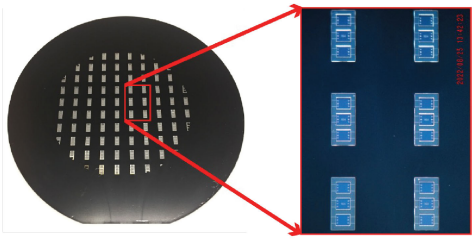

Fig. 15. Molded wafer with through-polymer rims (TPRs) that prevent EMC from covering the bonding pads.

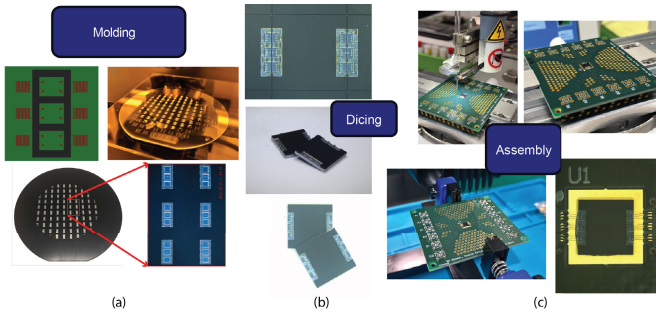

Fig. 16. (a) Wafer molding process. (b) Dicing process. (c) Wire bonding of the chip to the PCB.

III. Measurement and Experimental Results

A. Assembly Process and Measurement Setup

Nine 100-mm wafers were processed, each corresponding to a specific design, as shown in Fig. 4. After molding, the wafers were diced along the TPRs to optimize the length of the bond wires. The steps of molding, dicing, and assembly are illustrated sequentially in Fig. 16.

To prepare the measurement setup, a PCB was designed using Altium Designer and manufactured by Eurocircuits N.V., a company specializing in PCB manufacturing in Belgium. The design considers numerous holes on the surface of the PCB, so the humidity can flow around the chip more efficiently. Moreover, SMB connectors have been used in order to reduce noise and enhance the accuracy of the capacitance measurements. The final device wirebonded to the PCB is illustrated in Fig. 17.

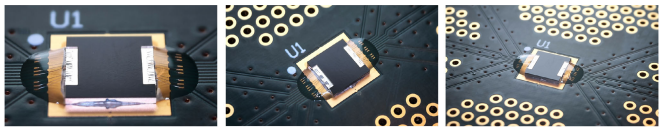

Fig. 17. Final DUT with the wire-bonded chip mounted on the PCB.

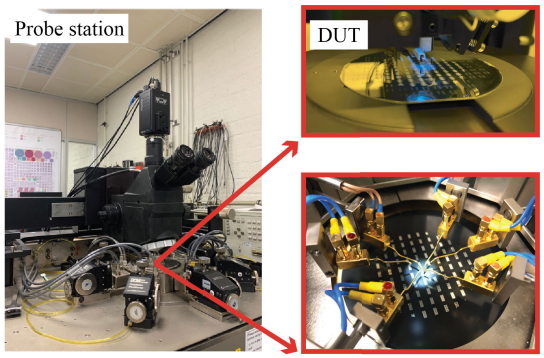

Fig. 18. (a) Semiautomatic probe station. (b) Device under test (DUT) [17].

B. Results and Discussion

The manufactured wafer comprises 70 dies (6 mm × 6 mm). Each die contains six capacitive sensors. Each sensor covers an area of 480 μm × 620 μm. Before running the experiments, the nominal capacitance of the device is measured using a wafer-scale semiautomatic probe station, which is shown in Fig. 18. The capacitance was measured before and after molding, extracting the equivalent parallel capacitance, parallel conductance, and parasitic capacitance.

For example, MS1 exhibited capacitance values of 1.54 pF before molding and 5.85 pF after molding. A similar trend was observed for other sensors. The relative dielectric constant is increased by approximately a factor of 4 after EMC molding. Furthermore, Fig. 19 illustrates the tolerance of the MS4 capacitance under varying bias voltages. The capacitance remains stable within the range of 5.85–5.86 pF, with a variation of less than 7 aF, demonstrating its stability and robustness. A similar trend was observed for other sensors.

Before molding, no short circuits were detected in the fabrication yield. However, postmolding inspection revealed a few devices with shorted metal electrodes. These short circuits are likely caused by EMC flow between the metal fingers during molding, resulting in cracks or direct electrical contact between adjacent conductors. The results and processing yields are summarized in Table I.

To measure real-time capacitance, the Smartec universal transducer interface (UTI) has been employed. The UTI chip

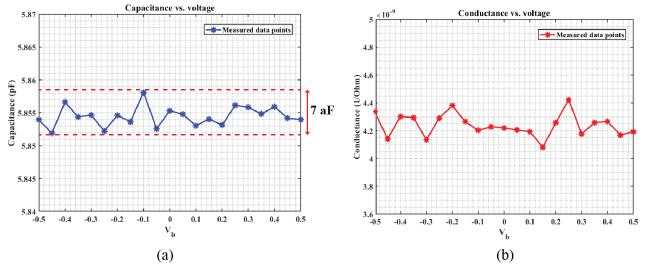

Fig. 19. MS4 calibration after molding. (a) Parallel capacitance. (b) Parallel conductance [17].

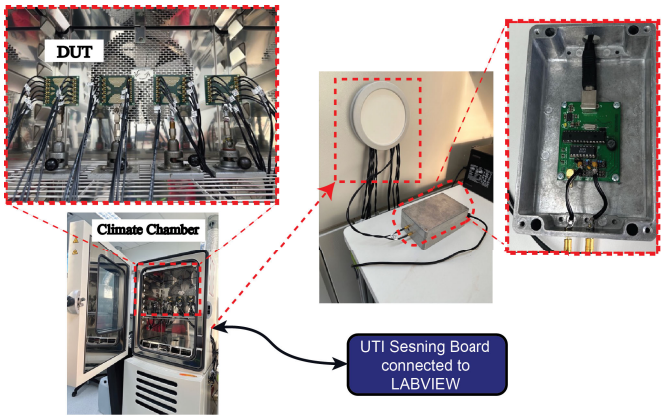

Fig. 20. Experimental setup inside the climate chamber with the device under test connected to the UTI evaluation board via SMB cables. The UTI PCB interfaces with LabVIEW for sensor readout.

used in the evaluation board is the UTI-1610-21914-0177-E-1123 model [17]. This evaluation board is an analog front end designed in [18] to interface directly with various passive sensors, including capacitive types. It converts low-level sensor signals into a period-modulated signal compatible with microcontrollers, enabling accurate measurements without the need for additional electronics [19]. In our experiment setup, shown in Fig. 20, the UTI board was confined to a metal box, which eliminates ambient noise and improves measurement accuracy. The UTI board interfaces with LabVIEW for automated measurements and signal processing.

The humidity experiments were conducted using the Vötschtechnik ClimeEvent C/180/70/3, a compact climate chamber designed for precise environmental testing [20]. The climate chamber is equipped with reference sensors to accurately measure both temperature and humidity. These integrated sensors enable the chamber to maintain and monitor the desired environmental conditions during testing. We conduct in situ reliability experiments by setting the temperature and humidity of the chamber to specific values and then observing the sensor's behavior over a sufficient period to ensure that the EMC absorbs the humidity and reaches equilibrium, allowing the sensor output to stabilize. We then gradually increase the humidity and take measurements until we reach the maximum limit of the climate chamber's range. Afterward, we return to the starting point and observe the sensor output to assess the hysteresis behavior.

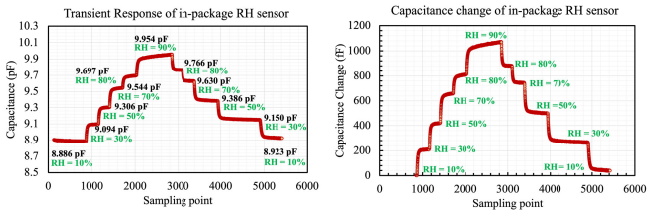

Fig. 21. Transient response of sensor MS5 with heterogeneous electrodes.

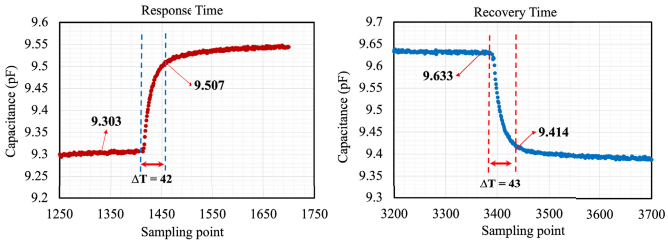

Fig. 22. (a) Response time. (b) Recovery time of sensor MS5 with heterogeneous electrodes.

The in-package sensor is specifically designed and manufactured to monitor the reliability of the packaging material (EMC). To evaluate its performance, nine chips with different layouts (MS1 to MS9), each comprising six sensors, were prepared and subjected to calibration tests for in situ reliability monitoring in the climate chamber. We exposed the packaged sensors to controlled RH levels of 10%–90% and temperature range of 10 °C–50 °C in the climate chamber. The RH range was chosen based on the standard operating conditions of the equipment. The temperature was set to 50 °C to access the full RH range, while measurements at room temperature limit the RH range to above 50%. The SMB cables, twisted in pairs, connected the measurement board to the sensor PCB inside the climate chamber, as shown in Fig. 20. Each measurement point took several hours to ensure that the water diffusion process was complete and the capacitance value stabilized. The RH and temperature of the chamber were recorded and controlled precisely using reference sensors located inside the chamber. The transient response of sensor MS5 with heterogeneous electrodes is shown in Fig. 21. The measurement was conducted by sweeping the RH from 10% to 90% and then returning to 10%. During this period, we observed stable results with no deviation from the expected trend in the sensor outputs. The response time and the recovery time of the sensor are illustrated in Fig. 22(a) and (b), respectively. However, the transient response does not reflect the in-package sensor's actual response time, as humidity absorption in the 200-μm EMC is slow to reach the sensor's active area. The reported response and recovery times only represent the water diffusion process in the EMC, not the sensor's speed.

The recorded data were analyzed using a LabVIEW program. Real-time capacitance measurements were collected with an approximate sampling time of 66 ms. The program averaged the data over each ten sampling points and reported

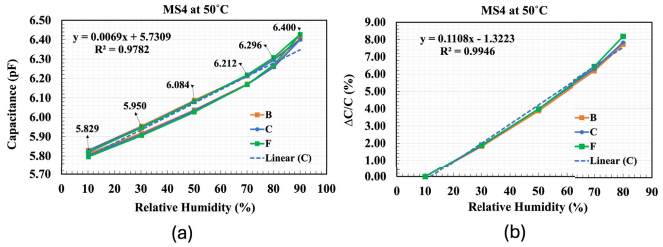

Fig. 23. (a) Capacitance measurement results of the sensor MS4 with uniform electrodes in a climate chamber under varying RH. (b) Relative capacitance change.

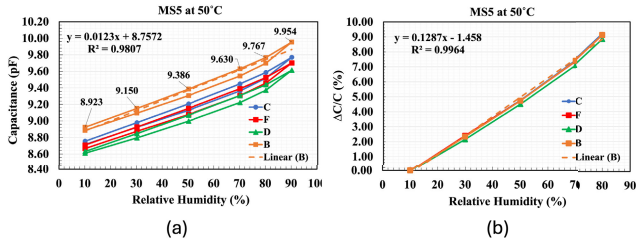

Fig. 24. (a) Capacitance measurement results of the sensor MS5 with heterogeneous electrodes in a climate chamber under varying RH. (b) Relative capacitance change.

real-time and average capacitance values, chamber temperature, and RH over time. The average data showed a standard deviation of 1–5 fF.

The performance of sensors with uniform and heterogeneous electrode designs is summarized in Table I. Sensors are compared based on their measured sensitivity, as defined in (2). The sensitivity values are extracted from the average experimental data and the linear fit equations obtained from the measurements. The values are used to evaluate the improvement achieved by the proposed design. A total of 54 sensors were measured, showing the expected trend and confirming the reproducibility and robustness of the design. Some samples were excluded from the analysis due to short connections that occurred during the molding process, as previously described. The measurement results shown in Figs. 23 and 24 confirm the higher sensitivity of the sensor with heterogeneous electrodes, with the sensitivity improving from 6.9 to 12.3 fF/%RH. The results also include the relative capacitance change versus RH and the corresponding linear fit equations, demonstrating a 20% increase in relative capacitance change. The total capacitance change over the measured humidity range reached a significant value of more than 1 pF

$$\text{Sensitivity} = \frac{\Delta C}{\Delta \text{RH}(\%)}. \tag{2}$$

The hysteresis behavior is evaluated in Figs. 23(c) and 24(c). As can be seen in the RH level of 80%–90%, nonlinearity has been observed at the data points. This deviation from linearity is probably attributed to the substantial swelling of the sensing material as a result of water absorption. This effect has been verified using the mass measurement of the devices under test, as reported in Fig. 25.

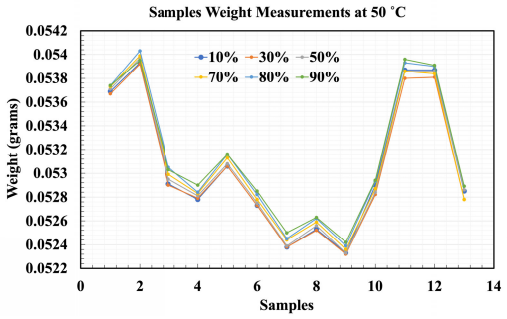

Fig. 25. Mass measurements of bare dies at 50 °C.

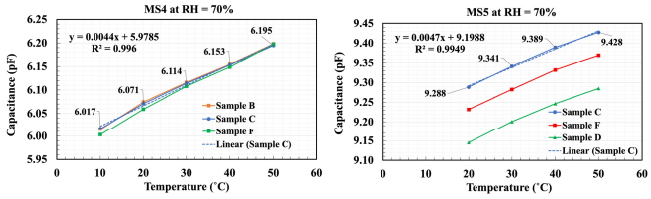

Fig. 26. MS4 and MS5 capacitance variation with temperature.

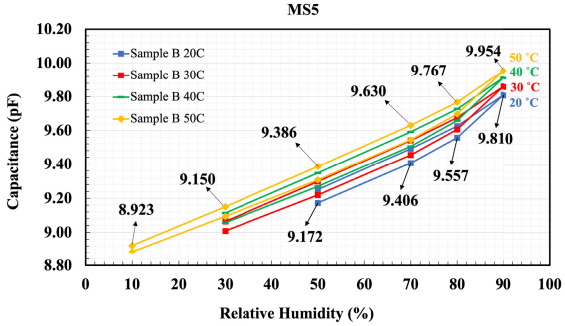

Fig. 27. MS5 sensor's behavior under varying RH levels at different temperatures.

MS1 exhibits higher sensitivity due to its finer pitch and width (1 μm), maximizing the capacitance value within a given area. However, a fair comparison with the heterogeneous design having the same pitch would result in improved sensitivity by optimizing the electrode geometry, enabling more efficient use of the electric field. In addition, temperature effects should be studied to ensure a consistent linear response, allowing for proper calibration during reliability tests. To verify this, the capacitance at 70% RH was monitored while the temperature varied within the range of 10 °C–50 °C. This temperature range is achievable only when RH is above 70% under standard operating conditions. The effect of temperature on the performance of MS4 and MS5 are reported in Figs. 26 and 27. The behavior of the MS5 sensor is recorded at room temperature, with additional curves at higher temperatures. The proposed device supports a wide temperature range, as it is CMOS-compatible, has no active components, and relies on electrostatic sensing, functioning within the full CMOS package limits. After calibration, the sensor enables reliability monitoring by measuring its

capacitance, which directly reflects the relative humidity level and moisture content within the package.

IV. Conclusion

Unlike conventional humidity sensors that measure ambient RH, the proposed in-package RH sensor provides real-time data on EMC moisture content, making it easier to assess package reliability over time.

The design directly uses EMC as the sensing layer, encapsulating the electrodes during standard packaging. To improve sensitivity, a heterogeneous electrode design is introduced. By carefully controlling the etching time with BHF, the oxide under the narrower electrode sections is fully removed, while the wider sections remain supported by oxide pillars. This creates semifloating electrodes, allowing EMC to completely surround the etched regions. As a result, more electric field lines pass through the sensing material, improving sensitivity and ensuring accurate moisture detection.

Experimental results show that the proposed sensor outperforms existing solutions. A comparison between the uniform IDE design (MS4) and the new heterogeneous design (MS5) confirms that the sensitivity increased from 6.9 to 12.3 fF/%RH, with a 20% increase in relative capacitance change.

The proposed in-package test sensor can be further optimized for packaging reliability tests. Its CMOS compatibility allows integration with CMOS electronics for system-in-package (SiP) reliability monitoring. The sensor can be fabricated with different epoxy compounds, enabling broader material studies and applications across various packaging technologies. In addition, the sensor can also contribute to studying EMC aging and RF applications, where dielectric constant changes affect signal attenuation, offering insights into semiconductor package reliability under RF stress. Sensitivity can be further improved by refining the electrode design with finer features and an asymmetric heterogeneous structure to enhance electric field confinement. The proposed sensor can also be monolithically integrated with the thermal test chip (TTC) in [21] and [22] to support multidomain reliability testing, where the TTC's temperature sensor can compensate for RH sensor drift.

Acknowledgment

The authors thank Arnold Bos and Ton van Weelden from Boschman B.V., The Netherlands, for their invaluable contributions and support in providing wafer molding technology. The Boschman B.V. team provided the molding process with a thickness of 200 μm, which was executed locally using through-polymer rims (TPRs).

References

[1] J. Chen, Q. Nguyen, J. C. Roberts, J. C. Suhling, R. C. Jaeger, and P. Lall, "Moisture-induced die stresses in PBGA packages exposed to various environments," presented at the 17th IEEE Intersociety Conf. Thermal Thermomechanical Phenomena Electron. Syst. (ITherm), San Diego, CA, USA, May 2018.

[2] Q. Nguyen, J. C. Roberts, J. C. Suhling, and R. C. Jaeger, "Measurement and simulation of moisture induced die stresses in quad flat packages," presented at the 15th IEEE Intersociety Conf. Thermal Thermomechanical Phenomena Electron. Syst. (ITherm), May 2016.

[3] X. Fan and V. Nagaraj, "In-situ moisture desorption characterization of epoxy mold compound," in *Proc. 13th Int. Thermal, Mech. Multi-Phys. Simulation Exp. Microelectron. Microsyst.*, Apr. 2012, pp. 1/6–6/6.

[4] C.-L. Dai, "A capacitive humidity sensor integrated with micro heater and ring oscillator circuit fabricated by CMOS–MEMS technique," *Sens. Actuators B, Chem.*, vol. 122, no. 2, pp. 375–380, Mar. 2007.

[5] S. Chen, V. P. J. Chung, D. Yao, and W. Fang, "Vertically integrated CMOS-MEMS capacitive humidity sensor and a resistive temperature detector for environment application," in *Proc. 19th Int. Conf. Solid-State Sensors, Actuators Microsyst. (TRANSDUCERS)*, Jun. 2017, pp. 1453–1454.

[6] C.-Y. Lee and G.-B. Lee, "Humidity sensors: A review," *Sensor Lett.*, vol. 3, nos. 1–2, pp. 1–15, 2005.

[7] Z. Chen and C. Lu, "Humidity sensors: A review of materials and mechanisms," *Sensor Lett.*, vol. 3, no. 4, pp. 274–295, 2005.

[8] C.-L. Zhao, M. Qin, and Q.-A. Huang, "A fully packaged CMOS interdigital capacitive humidity sensor with polysilicon heaters," *IEEE Sensors J.*, vol. 11, no. 11, pp. 2986–2992, Nov. 2011.

[9] T. A. Blank, L. P. Eksperiandova, and K. N. Belikov, "Recent trends of ceramic humidity sensors development: A review," *Sens. Actuators B, Chem.*, vol. 228, pp. 416–442, Jun. 2016.

[10] P. J. Schubert and J. H. Nevin, "A polyimide-based capacitive humidity sensor," *IEEE Trans. Electron Devices*, vol. ED-32, no. 7, pp. 1220–1223, Jul. 1985.

[11] J. Boudaden et al., "Polyimide-based capacitive humidity sensor," *Sensors*, vol. 18, no. 5, p. 1516, May 2018.

[12] H. Liu et al., "Humidity sensors with shielding electrode under interdigitated electrode," *Sensors*, vol. 19, no. 3, p. 659, Feb. 2019.

[13] R. Sattari, H. v. Zeijl, and G. Zhang, "Manufacturing of an in-package relative humidity sensor for epoxy molding compound packages," in *Proc. 24th Int. Conf. Thermal, Mech. Multi-Phys. Simulation Exp. Microelectron. Microsyst. (EuroSimE)*, Apr. 2023, pp. 1–6.

[14] S. Fujita and Y. Kamei, "Electrical properties of polyimide with water absorption," in *Proc. 11th Int. Symp. Electrets*, Oct. 2002, pp. 275–278.

[15] R. Sattari, H. van Zeijl, and G. Zhang, "Design and manufacturing of an in-package relative humidity sensor with multi-width interdigital electrodes towards enhanced sensitivity for characterization of packaging encapsulation materials," in *Proc. IEEE 25th Electron. Packag. Technol. Conf. (EPTC)*, Dec. 2023, pp. 588–591.

[16] Kayaku Advanced Materials Inc. *SU-8 3050: Negative Photoresist*. Kayaku Adv. Mater. Inc. Accessed: Jan. 20, 2024. [Online]. Available: https://kayakuam.com/wp-content/uploads/2020/07/KAM-SU-8-3000-Datasheet-7.10-final.pdf

[17] Angst+Pfister. *UTI_1610-21914-0177-E-1123 Datasheet*. Angst+Pfister. Accessed: Sep. 15, 2024. [Online]. Available: https://sensorsandpower.angst-pfister.com/fileadmin/products/datasheets/183/UTI_1610-21914-0177-E-1123.pdf

[18] F. M. L. van der Goes, "Low-cost smart sensor interfacing," Ph.D. dissertation, Dept. Elect. Eng., Mathematics Comput. Sci., Delft Univ. Technol., Delft, The Netherlands, Apr. 1996. [Online]. Available: https://repository.tudelft.nl/record/uuid:1f573140-ddc2-4dc7-b7c4-9db673bd17af

[19] Smartec B.V. *Universal Transducer Interface (UTI) Datasheet*. Smartec B.V. [Online]. Available: https://cdn.soselectronic.com/productdata/11/ac/19506ca7/uti-kit-evb-board-utikit.pdf

[20] Vötschtechnik. (2025). *ClimeEvent C/180/70/3 Climate Test Chamber*. [Online]. Available: https://backend.weiss-technik.com/webapp/weisstechnik/products/environmental-simulation/climate-test-chambers-type-climeevent/weisstechnik-ClimeEvent-EN.pdf

[21] R. Sattari, H. van Zeijl, and G. Zhang, "Design and fabrication of a multi-functional programmable thermal test chip," in *Proc. 23rd Eur. Microelectron. Packag. Conf. Exhib. (EMPC)*, Sep. 2021, pp. 1–7.

[22] R. Sattari, D. Hu, X. Liu, H. van Zeijl, S. Vollebregt, and G. Zhang, "Transient thermal measurement on nano-metallic sintered die-attach joints using a thermal test chip," *Appl. Thermal Eng.*, vol. 221, Feb. 2023, Art. no. 119503.

Romina Sattari (Member, IEEE) was born in Tehran, Iran, in 1993. She received the B.Sc. and M.Sc. degrees in electrical engineering from the Sharif University of Technology, Tehran, in 2015 and 2017, respectively. She is now pursuing the Ph.D. degree with the Electronic Components, Technology and Materials (ECTM) Group, Delft University of Technology (TUD) Delft, Delft, The Netherlands.

Her M.Sc. thesis focused on indoor positioning systems and RF transceivers and Ph.D. research focused on multidomain reliability monitoring of semiconductor packages and modules. During her Ph.D. study, she designed and fabricated various in-package sensors and smart chips for the characterization and qualification of materials and semiconductor packages. She is currently a Staff Member at the Department of Microelectronics and an IC Design Support Specialist at the Faculty of EEMCS, TUD, while continuing her research on in-package reliability sensors and contributing to various projects at TU Delft.

Henk van Zeijl received the Ph.D. degree from Delft University of Technology (TUD), Delft, The Netherlands, in 2005.

He joined TUD, in 1980, where he worked in the field of neutron diffraction and instrumental neutron activation analysis. In 1986, he joined Delft Institute of Microelectronics and Submicron Technology (DIMES). From 1989 to 1998, he was responsible for mask fabrication and lithography in the DIMES IC process research sector. He developed several technology courses and a full week of training for engineers from relevant fields in the industry and academia. Since 2007, he has been a part-time Teacher and an Advisor for M.Sc. and Ph.D. students. Besides these educational activities, he cooperated in different research projects related to lithography, MEMs, 3-D integration, packaging, and solid-state lighting integration. Since August 2017, he has been a Staff Member at the Laboratory of Electronic Component Technology and Materials (ECTM), Delft. He is the (co-)author of more than 80 technical articles and several patents.

Dr. van Zeijl is a member of the IEEE Electronics Packaging Society/Power Electronics Society.

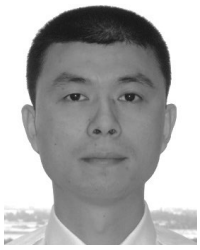

Zu Yao Chang (Member, IEEE) received the M.Sc. degree in electrical engineering from Delft University of Technology, Delft, The Netherlands, in 2003.

Since 2003, he has been a Staff Member with the Electronic Instrumentation Laboratory, Delft University of Technology, working on impedance measurement systems and smart sensor systems.

Guo Qi Zhang (Fellow, IEEE) is a member of Netherlands Academy of Engineering, the Chair Professor of "Micro/Nanoelectronics System Integration and Reliability" at Delft University of Technology (TUD), Delft, The Netherlands. Before joining TUD, he worked for NXP, Eindhoven, The Netherlands, and Philips, Eindhoven, as a Senior Director of Technology Strategy and a Research Fellow until 2013. His research interests cover multilevel heterogeneous system integration and packaging; multiphysics and multiscale modeling and optimization of micro/nanoelectronics; digital twin and designing for reliability; and wide bandgap semiconductors sensors and components and SSL technology.

Dr. Zhang received the IEEE Technical Field Award on packaging. Currently, he serves as a Secretary-General for IEEE the International Technology Roadmap of Wide Bandgap Power Semiconductors (ITRW). He chaired the "More than Moore" of European's technology platform for micro/nanoelectronics and served as the Co-Chair for the academic council of Dutch national innovation program on microelectronics/nanoelectronics and embedded systems. He was the Founding Person for MEMSLand, the NL National MEMS Research Consortium.